2024 IEEE 63rd Conference on Decision and Control (CDC)
December 16-19, 2024. MiCo, Milan, Italy

Robust Global Attitude Tracking on $\mathrm{SO}(3)$ via MRP-based hybrid feedback

Luís Martins, Carlos Cardeira, and Paulo Oliveira

***Abstract*— This paper introduces an innovative control solution to tackle the problem of robust attitude tracking for fully actuated rigid bodies. The approach resorts to the modified Rodrigues parameters (MRP), whose configuration manifold is a double cover of the three-dimensional rotation group, to design a dynamic hybrid controller that yields uniform global asymptotic and semi-global exponential tracking results in the covering space. The controller includes an integral term to deal with constant disturbances and a smoothing mechanism to generate a jump-free control signal. By relying on a hybrid dynamic path-lifting algorithm and novel equivalence of stability concepts, the authors demonstrate that the MRP-based dynamic controller globally asymptotically and semi-globally exponentially stabilizes the tracking dynamics in the base space $\mathrm{SO}(3)$ with robustness to small measurement noise and unknown fixed disturbances. The simulation results showcase the performance of the proposed hybrid controller.**

I. INTRODUCTION

A. Motivation and Literature Review

Rigid body attitude control is an active area of research aimed at developing precise and robust control algorithms to track or stabilize the attitude dynamics of a rigid body, finding widespread application in diverse fields, such as robotics systems and aircraft, spacecraft, and underwater vehicles [1]. However, designing these control strategies is inherently complex due to the nonlinear dynamics and the topological obstruction of the rotation group space [2].

The topological obstruction precludes solving the attitude control problem globally with a smooth feedback law, yielding, at best, an almost global stability result [3]. Furthermore, the obstruction also prevents the robust global asymptotic stabilization of the attitude dynamics through discontinuous feedback [4]. Thus, to bypass these particularities of the configuration manifold and achieve both robust and global results, the design within the hybrid systems framework is frequently adopted ([3], [5], [6], [7], [8], [9]).

The hybrid solutions can be differentiated based on the attitude representation resorted. Concerning solutions devised directly on the three-dimensional special orthogonal group $\mathrm{SO}(3)$, in [3], [5], [6], the authors propose hybrid methodologies relying on a family of potential functions. The solution reported in [3] includes an integral action and achieves robust global exponential stability in the presence of fixed disturbances for the attitude tracking dynamics. In [5], [6], the solutions encompass distinct smoothing mechanisms to remove the discontinuities from the control signal and yield, respectively, robust global asymptotic and global exponential tracking properties. A hybrid strategy using a single potential function on $\mathrm{SO}(3)$ and equipped with a smoothing mechanism has been proposed in [8], leading to global asymptotic tracking and semi-global exponential tracking properties. Another relevant approach consists of developing a hybrid feedback using local coordinates in a covering space of $\mathrm{SO}(3)$, such as unit quaternions [9], [10] or MRP ([11], [12], [13]). The hybrid formulation enables overcoming the unwinding phenomenon, which is an undesirable behavior susceptible to occur when relying on a multiple covering of the rotation group [10]. The MRP-based solution proposed in [12] semi-globally exponentially stabilizes, with nominal robustness to small perturbations, the attitude tracking dynamics on a covering manifold of $\mathrm{SO}(3)$. However, to directly translate these controllers and the respective asymptotic/exponential tracking properties to $\mathrm{SO}(3)$, these methodologies must be paired with a hybrid dynamic path-lifting system [10], [14].

B. Contributions

This paper proposes a novel approach to the attitude tracking problem for fully actuated rigid bodies. First, a dynamic hybrid feedback controller is designed in the MRP space. This controller extends the semi-global exponential attitude tracking solution reported in [12] by including an integral action and a smoothing mechanism. In this way, while preserving the exponential tracking property, the resulting hybrid scheme deals effectively with fixed disturbances and yields an actuation devoid of discontinuities induced by the MRP switching. The output of the controller, apart from a simple feedforward canceling term, only comprises linear terms and does not have restrictive constraints on the gains, leaving the achievable performance unaffected. Then, by resorting to the path-lifting algorithm proposed in [14] to uniquely and consistently extract the MRP from the rotation matrix error, the MRP-based hybrid feedback is applied to the actual rigid body attitude space tracking dynamics. The main contribution of this work is the global asymptotic and semi-global exponential tracking results on $\mathrm{SO}(3)$ with robustness to fixed disturbances and any small perturbations obtained with the resulting closed-loop hybrid system. Compared to the rotation group $\mathrm{SO}(3)$, or even the

L. Martins is with the Institute of Mechanical Engineering, Instituto Superior Técnico, Universidade de Lisboa, Lisboa, Portugal luis.cunha.martins@tecnico.ulisboa.pt

C. Cardeira is with the Institute of Mechanical Engineering, Instituto Superior Técnico, Universidade de Lisboa, Lisboa, Portugal carlos.cardeira@tecnico.ulisboa.pt

P. Oliveira is with the Institute of Mechanical Engineering and the Institute for Systems and Robotics, Instituto Superior Técnico, Universidade de Lisboa, Lisboa, Portugal paulo.j.oliveira@tecnico.ulisboa.pt

unit quaternion space $\mathbb{S}^3$, the MRP configuration manifold has a less complex structure, requiring fewer parameters and verifying fewer constraints to describe its elements. Thus, the approach simplifies the hybrid control design. Furthermore, the MRP representation has the particularity of the triplet with the smallest norm always describing the shortest principal rotation [15]. The methodology exploits this unique characteristic to circumvent the *unwinding phenomenon* without relying on additional control states, as required in quaternion-based strategies ([9], [10]). Compared to synergistic hybrid approaches ([3], [6]), leveraging these properties results in a simpler architecture that eliminates the need for formulating multiple potential functions. Moreover, compared to the single potential function approach [8], which relies on a hybrid auxiliary scalar variable, the MRP-based controller does not have supplementary variables and the memory states of the path-lifting mechanism are strictly discrete. To the authors' best knowledge, the approach of this paper is the first robust semi-global exponential stability result in the rigid-body attitude configuration space using a hybrid controller designed on a covering manifold of $\mathrm{SO}(3)$.

C. Organization

The paper is organized as follows: section II introduces the notation and some key concepts on attitude representations and dynamical hybrid systems; section III presents the underlying attitude rigid-body dynamic model and formulates the control objective; section IV addresses the design of a hybrid dynamic controller to uniformly globally asymptotically and semi-globally exponentially stabilize the attitude dynamics in the covering space; section V explores an equivalence of stability framework to yield robust global asymptotic and semi-global exponential tracking results in the base space; section VI displays and analyzes the simulation responses; section VII concludes the paper with closing remarks.

II. Notation and Preliminaries

A. Notation

Throughout this work, $\mathbb{R}$, $\mathbb{R}_{\geq 0}$, $\mathbb{R}_{>0}$, and $\mathbb{N}$ express the set of real, positive real, nonnegative real, and natural numbers, respectively; $\mathbb{R}^n$ represents the n-dimensional Euclidean space; $K\mathbb{B}^n$ denotes the closed ball of radius $K \in \mathbb{R}_{>0}$ centered at the origin of $\mathbb{R}^n$; $\mathbb{R}^{n\times m}$ denotes the set of $n \times m$ matrices; $\mathbb{R}^{n\times n}_{\succ 0}$ represents the set of $n \times n$ positive definite matrices; $\mathbb{S}^n = \left\{\mathbf{x} \in \mathbb{R}^{n+1} : \mathbf{x}^\top \mathbf{x} = 1\right\}$ symbolizes the n-dimensional unit sphere; $\bar{\mathbb{R}}^n = \mathbb{R}^n \cup \{\infty\}$ denotes the Alexandroff compactification of $\mathbb{R}^n$ [16, p. 246]; $\mathbf{I_n} \in \mathbb{R}^{n\times n}$ represents the n-dimensional identity matrix; $\mathbf{F} : \mathcal{X} \rightrightarrows \mathcal{Y}$ represents the set-valued map $\mathbf{F}$ from $\mathcal{X}$ to $\mathcal{Y}$ and, for $\mathbf{x} \in \mathcal{X}$, the relation $\dot{\mathbf{x}} \in \mathbf{F}(\mathbf{x})$ expresses a differential inclusion; dom $\mathbf{V}$ symbolizes the domain of the function $\mathbf{V} : \mathbb{R}^m \mapsto \mathbb{R}^n$; $\mathbf{e_i} \in \mathbb{R}^3$ denotes a vector of zeros except for the i$^{\text{th}}$ entry which is 1; the operator $[\cdot]_\times : \mathbb{R}^3 \mapsto \{\mathbf{S} \in \mathbb{R}^{3\times 3} : \mathbf{S}^\top = -\mathbf{S}\}$ is such that $[\omega]_\times s = \boldsymbol{\omega} \times \mathbf{s}$ for any $\mathbf{s}, \boldsymbol{\omega} \in \mathbb{R}^3$, where $\times$ denotes the cross product [10]; for $\mathbf{s} \in \mathbb{R}^n$, $\|\mathbf{s}\|$ is the Euclidean norm. For a given square matrix $\mathbf{A} \in \mathbb{R}^{n\times n}$, $\lambda_{\min}(\mathbf{A})$ and $\lambda_{\max}(\mathbf{A})$ denote the minimum and maximum eigenvalues, respectively; $\|\mathbf{A}\| = (\lambda_{max}(\mathbf{A}^\top \mathbf{A}))^{1/2}$ corresponds to the spectral norm; $\mathrm{diag}\,(\mathbf{s})$ is such that $\mathrm{diag}\,(\mathbf{s}) \triangleq \sum_{i=1}^n (\mathbf{e_i}\mathbf{e_i}^\top)(\mathbf{e_i}^\top \mathbf{s})$ for $\mathbf{s} \in \mathbb{R}^n$. The saturation function here considered is aligned with the following definition.

Definition 1: The function $\sigma : \mathbb{R} \mapsto \mathbb{R}$ is smooth, odd, and verifies: (1) $\sigma(0) = 0$; (2) $s\sigma(s) > 0 \;\; \forall \;\; s \neq 0$; (3) $\lim_{s\to\pm\infty} \sigma(s) = \pm M$, with $M > 0$; (4) $0 < \dot{\sigma}(s) \leq 1$. $\square$

B. Attitude Representation

The three-dimensional special orthogonal group $\mathrm{SO}(3) := \{\mathbf{R} \in \mathbb{R}^{3\times 3} : \mathbf{R}^\top \mathbf{R} = \mathbf{I_3}, \det(\mathbf{R}) = 1\}$ is the configuration manifold for the attitude of a rigid body. Consider a body-fixed frame and an inertial frame, $\mathbf{R} \in \mathrm{SO}(3)$ denotes a given element of this boundaryless compact manifold and represents the rotation matrix from the former to the latter frame. The unit quaternion attitude representation links each element $\mathbf{R} \in \mathrm{SO}(3)$ with two vectors of $\mathbb{S}^3$. Specifically, a given $\mathbf{q} := (q_0, \mathbf{q_1}) \in \mathbb{S}^3$ denotes the unit quaternion, where $q_0 \in \mathbb{R}$ and $\mathbf{q_1} \in \mathbb{R}^3$ are the scalar and vector components, respectively, and is associated with a rotation matrix $\mathbf{R}$ of $\mathrm{SO}(3)$ through the map $\mathcal{R} : \mathbb{S}^3 \mapsto \mathrm{SO}(3)$ defined as

$$\mathcal{R}(\mathbf{q}) = \mathbf{I_3} + 2q_0\,[\mathbf{q_1}]_\times + 2\,[\mathbf{q_1}]_\times^2\,,$$

which satisfies $\mathcal{R}(\mathbf{q}) = \mathcal{R}(-\mathbf{q})$ [10, Eq. 5]. The double-valued inverse map $\mathcal{Q} : \mathrm{SO}(3) \rightrightarrows \mathbb{S}^3$ is described by

$$\mathcal{Q}(\mathbf{R}) = \{\mathbf{q} \in \mathbb{S}^3 : \mathcal{R}(\mathbf{q}) = \mathbf{R}\}.$$

The MRP result from the stereographic projection of the unit quaternion representation [15], providing an alternative rigid-body attitude description. Each MRP vector $\boldsymbol{\vartheta}$ has a shadow MRP associated, $\boldsymbol{\vartheta}^s \in \bar{\mathbb{R}}^3$. A given unit quaternion is related to $\boldsymbol{\vartheta}$ and $\boldsymbol{\vartheta}^s$ through the maps

$$\boldsymbol{\vartheta} = \boldsymbol{\varphi}(\mathbf{q}) = \begin{cases} \mathbf{q_1}(1+q_0)^{-1} & , \text{ for } \mathbf{q} \in \mathbb{S}^3 \setminus \{\mathbf{s}\} \\ \boldsymbol{\infty} & , \text{ for } \mathbf{q} = \mathbf{s} \end{cases}, \tag{1a}$$

$$\boldsymbol{\vartheta}^s = \boldsymbol{\varphi}(-\mathbf{q}) = \begin{cases} -\mathbf{q_1}(1-q_0)^{-1} & , \text{ for } \mathbf{q} \in \mathbb{S}^3 \setminus \{\mathbf{n}\} \\ \boldsymbol{\infty} & , \text{ for } \mathbf{q} = \mathbf{n} \end{cases}, \tag{1b}$$

where $\mathbf{s} = (-1, 0, 0, 0)$ and $\mathbf{n} = (1, 0, 0, 0)$. The stereographic projection $\boldsymbol{\varphi} : \mathbb{S}^3 \mapsto \bar{\mathbb{R}}^3$ and its inverse mapping $\boldsymbol{\varphi}^{-1} : \bar{\mathbb{R}}^3 \mapsto \mathbb{S}^3$ are smooth [14]. Since the MRP sets are singular for different rotations, judiciously alternating between them gives rise to a minimal non-singular attitude representation [15]. The map $\boldsymbol{\Upsilon} : \bar{\mathbb{R}}^3 \mapsto \bar{\mathbb{R}}^3$, given by

$$\boldsymbol{\vartheta^s} = \boldsymbol{\Upsilon}(\boldsymbol{\vartheta}) = \begin{cases} -\boldsymbol{\vartheta}\|\boldsymbol{\vartheta}\|^{-2} & , \text{ for } \boldsymbol{\vartheta} \in \mathbb{R}^3 \setminus \{\mathbf{0}\} \\ \boldsymbol{\infty} & , \text{ for } \boldsymbol{\vartheta} \in \{\mathbf{0}\} \\ \mathbf{0} & , \text{ for } \boldsymbol{\vartheta} \in \{\boldsymbol{\infty}\} \end{cases},$$

enables obtaining the shadow MRP from the original MRP. Both MRP triplets satisfy the differential equation [15]

$$\dot{\boldsymbol{\vartheta}} = \mathbf{T}(\boldsymbol{\vartheta})\boldsymbol{\omega} = \begin{cases} \frac{(1-\|\boldsymbol{\vartheta}\|^2)\mathbf{I_3} + 2[\boldsymbol{\vartheta}]_\times + 2\boldsymbol{\vartheta}\boldsymbol{\vartheta}^\top}{4}\boldsymbol{\omega}, & \text{for } \boldsymbol{\vartheta} \in \mathbb{R}^3 \\ \boldsymbol{\infty} & , \text{ for } \boldsymbol{\vartheta} \in \{\boldsymbol{\infty}\} \end{cases}. \tag{2}$$

The mapping $\mathcal{R}_{\boldsymbol{\vartheta}}(\boldsymbol{\vartheta}) : \bar{\mathbb{R}}^3 \mapsto \mathrm{SO}(3)$

$$\mathcal{R}_{\boldsymbol{\vartheta}}(\boldsymbol{\vartheta}) := \begin{cases} \mathbf{I_3} + \frac{8[\boldsymbol{\vartheta}]_\times^2 - 4(1-\|\boldsymbol{\vartheta}\|^2)[\boldsymbol{\vartheta}]_\times}{(1+\|\boldsymbol{\vartheta}\|^2)^2} & , \text{ for } \boldsymbol{\vartheta} \in \mathbb{R}^3 \\ \mathbf{I_3} & , \text{ for } \boldsymbol{\vartheta} \in \{\boldsymbol{\infty}\} \end{cases} \tag{3}$$

maps a given $\boldsymbol{\vartheta}$ to the equivalent $\mathbf{R}$ and verifies $\mathcal{R}_{\boldsymbol{\vartheta}}(\boldsymbol{\vartheta}) = \mathcal{R}_{\boldsymbol{\vartheta}}(\boldsymbol{\vartheta^s})$. For more insights on MRP, please see [15].

C. Hybrid Systems

The quadruplet $\mathcal{H} = (\mathbf{C}, \mathbf{F}, \mathbf{D}, \mathbf{G})$ encapsulates the fundamental elements of a hybrid system with the form

$$\mathcal{H}\begin{cases} \dot{\mathbf{x}} \in \mathbf{F}(\mathbf{x}) & , \quad \mathbf{x} \in \mathbf{C} \\ \mathbf{x}^+ \in \mathbf{G}(\mathbf{x}) & , \quad \mathbf{x}^+ \in \mathbf{D} \end{cases} . \tag{4}$$

The set-valued map $\mathbf{F} : \mathbb{R}^n \rightrightarrows \mathbb{R}^n$ governs the continuous evolution of $\mathcal{H}$ while in the flow set $\mathbf{C} \subset \mathbb{R}^n$, whereas the set-valued map $\mathbf{G} : \mathbb{R}^n \rightrightarrows \mathbb{R}^n$ dictates the discontinuous changes while in the jump set $\mathbf{D} \subset \mathbb{R}^n$. A solution $\mathbf{x}(t, j)$ to $\mathcal{H}$, with t and j denoting, respectively, ordinary and jump times, is a function $\mathbf{x} : \operatorname{dom} \mathbf{x} \mapsto \mathbb{R}^n$, where $\operatorname{dom} \mathbf{x} \subset \mathbb{R}_{\geq 0} \times \mathbb{N}$ is a hybrid time domain. A comprehensive perspective on hybrid systems can be found in [17].

III. Problem Statement

The underlying kinematic and dynamic equations for the rotation of a rigid body are, respectively,

$$\dot{\mathbf{R}} = \mathbf{R}\left[\boldsymbol{\omega}\right]_\times, \tag{5a}$$

$$\mathbf{J}\dot{\boldsymbol{\omega}} = \left[\mathbf{J}\boldsymbol{\omega}\right]_\times \boldsymbol{\omega} + \boldsymbol{\tau} + \mathbf{d}, \tag{5b}$$

where $\boldsymbol{\omega} \in \mathbb{R}^3$ symbolizes the angular velocity expressed in the body-fixed frame, $\boldsymbol{\tau} \in \mathbb{R}^3$ denotes the torque input, $\mathbf{J} \in \mathbb{R}^{3\times3}_{\succ 0}$ models the diagonal tensor of inertia of the rigid body, and $\mathbf{d} \in \mathbb{R}^3$ is an unknown fixed disturbance.

Let the map $\mathbf{r}(t) : \mathbb{R}_{\geq 0} \mapsto \boldsymbol{\Omega}$, given by $\mathbf{r}(t) := (\mathbf{R_d}, \boldsymbol{\omega}_\mathbf{d})(t)$, define the reference trajectory encompassing the desired rotation matrix, $\mathbf{R_d} \in \mathrm{SO}(3)$, and the desired angular velocity $\boldsymbol{\omega}_\mathbf{d} \in \mathbb{R}^3$. The subset $\boldsymbol{\Omega} \subset \mathrm{SO}(3) \times \mathbb{R}^3$ is compact and the trajectory $\mathbf{r}(t)$ is governed by

$$\dot{\mathbf{r}} \in \mathbf{F_r}(\mathbf{r}) := (\mathbf{R_d}[\boldsymbol{\omega}_\mathbf{d}]_\times, K_\omega \mathbb{B}^3) \quad \text{for} \quad \mathbf{r} \in \boldsymbol{\Omega}, \tag{6}$$

with $K_\omega \in \mathbb{R}_{>0}$. Every maximal solution $\mathbf{r}(t)$ to (6) is complete and, for any given $\mathbf{r}(t)$, $\boldsymbol{\omega}_\mathbf{d}$ is Lipschitz continuous with K_ω as Lipschitz constant [5]. With this definition in place, Problem 1 formulates the objective of this work.

Problem 1: Design a controller to render the compact set

$$\mathcal{A} = \{(\mathbf{r}, \mathbf{x}) \in \boldsymbol{\Omega} \times \boldsymbol{\chi} : \mathbf{R} = \mathbf{R_d}, \boldsymbol{\omega} = \boldsymbol{\omega}_\mathbf{d}\},$$

with $\mathbf{x} := (\mathbf{R}, \boldsymbol{\omega}) \in \boldsymbol{\chi} := \mathrm{SO}(3) \times \mathbb{R}^3$, robustly globally asymptotically and semi-globally exponentially stable for the attitude dynamic system (5). □

IV. MRP-based Global Exponential Control

Let $\tilde{\mathbf{R}} \in \mathrm{SO}(3)$ represent the rotation matrix error resulting from $\tilde{\mathbf{R}} = \mathbf{R_d}^\top \mathbf{R}$ and satisfying $\mathcal{R}_{\boldsymbol{\vartheta}}(\tilde{\boldsymbol{\vartheta}}) = \tilde{\mathbf{R}}$. To uniquely and consistently lift the MRP error representation $\tilde{\boldsymbol{\vartheta}}$ from the attitude error rigid body space, the approach relies on the hybrid dynamic path-lifting algorithm formulated in [14]. In this direction, consider the stereographic projection (1a) and let $m \in \{-1, 1\}$ and $\delta \in \mathbb{R}_{>0}$ be a discrete state and a hysteretic parameter, respectively. Consider also the vector $\mathbf{x_l} = (\hat{\mathbf{q}}, m, \tilde{\mathbf{R}}) \in \boldsymbol{\chi}_\mathbf{l} := \mathbb{S}^3 \times \{-1, 1\} \times \mathrm{SO}(3)$ to define the following flow and jump sets

$$\mathbf{C_m} := \{\mathbf{x_l} \in \boldsymbol{\chi}_\mathbf{l} : \|\boldsymbol{\varphi}(m\boldsymbol{\Phi}(\hat{\mathbf{q}}, \tilde{\mathbf{R}}))\| \leq 1 + \delta\},$$
$$\mathbf{D_m} := \{\mathbf{x_l} \in \boldsymbol{\chi}_\mathbf{l} : \|\boldsymbol{\varphi}(m\boldsymbol{\Phi}(\hat{\mathbf{q}}, \tilde{\mathbf{R}}))\| \geq 1 + \delta\},$$

where, as in [10], $\boldsymbol{\Phi} : \mathbb{S}^3 \times \mathrm{SO}(3) \rightrightarrows \mathbb{S}^3$ represents the map

$$\boldsymbol{\Phi}(\hat{\mathbf{q}}, \tilde{\mathbf{R}}) := \underset{\mathbf{p} \in \mathcal{Q}(\tilde{\mathbf{R}})}{\operatorname{argmax}} \quad \hat{\mathbf{q}}^\top \mathbf{p} \ , \tag{7}$$

and $\hat{\mathbf{q}} := (\hat{q}_0, \hat{\mathbf{q}}_\mathbf{1}) \in \mathbb{S}^3$ defines a memory state, whose update depends on the following flow and jump sets

$$\mathbf{C_q} := \{\mathbf{x_l} \in \boldsymbol{\chi}_\mathbf{l} : \operatorname{dist}(\hat{\mathbf{q}}, \mathcal{Q}(\tilde{\mathbf{R}})) \leq \alpha\},$$
$$\mathbf{D_q} := \{\mathbf{x_l} \in \boldsymbol{\chi}_\mathbf{l} : \operatorname{dist}(\hat{\mathbf{q}}, \mathcal{Q}(\tilde{\mathbf{R}})) \geq \alpha\},$$

with $\operatorname{dist}(\hat{\mathbf{q}}, \mathcal{Q}(\tilde{\mathbf{R}})) = \inf\left\{1 - \hat{\mathbf{q}}^\top \mathbf{p} : \mathbf{p} \in \mathcal{Q}(\tilde{\mathbf{R}})\right\}$ and $\alpha \in (0, 1)$. Then, the autonomous hybrid system $\mathcal{H}_\mathbf{l} := (\mathbf{C_l}, \mathbf{F_l}, \mathbf{D_l}, \mathbf{G_l})$, with the state $\mathbf{x_l} \in \boldsymbol{\chi}_\mathbf{l}$, the data

$$\mathbf{C_l} := \mathbf{C_q} \cap \mathbf{C_m}$$

$$\mathbf{F_l} := \begin{cases} \dot{\hat{\mathbf{q}}} = \mathbf{0} \\ \dot{m} = 0 \\ \dot{\tilde{\mathbf{R}}} \in \tilde{\mathbf{R}}\left[K_\omega^* \mathbb{B}^3\right] \end{cases}$$

$$\mathbf{D_l} := \mathbf{D_q} \cup \mathbf{D_m}$$

$$\mathbf{G_l} := \begin{cases} \hat{\mathbf{q}}^+ \in \boldsymbol{\Phi}(\hat{\mathbf{q}}, \tilde{\mathbf{R}}),\ m^+ = m, \text{ for } \mathbf{x_l} \in \mathbf{D_q} \\ \hat{\mathbf{q}}^+ = \hat{\mathbf{q}},\ m^+ = -m \ \ , \text{ for } \mathbf{x_l} \in \mathbf{D_m} \end{cases}, \tag{8a}$$

where $\dot{\tilde{\mathbf{R}}} \in \tilde{\mathbf{R}}\left[K_\omega^* \mathbb{B}^3\right]$ describes the dynamics of trajectories $\tilde{\mathbf{R}} : \mathbb{R}_{\geq} 0 \mapsto \mathrm{SO}(3)$ for some $K_\omega^* \in \mathbb{R}_{>0}$, and the output

$$\tilde{\boldsymbol{\vartheta}} := \begin{cases} \boldsymbol{\varphi}(m\boldsymbol{\Phi}(\hat{\mathbf{q}}, \tilde{\mathbf{R}})) & , \quad \mathbf{x_l} \in \mathbf{C_m} \cap \mathbf{C_q} \\ \emptyset & , \quad \mathbf{x_l} \notin \mathbf{C_m} \cap \mathbf{C_q} \end{cases},$$

describes the path-lifting mechanism for the MRP error extraction. As demonstrated in [14, Lemma 1], the output verifies the bound $\|\tilde{\boldsymbol{\vartheta}}\| \leq (1+\delta)$, i.e., its values are restricted to a three-dimensional unit sphere enveloped by a hysteresis layer whose thickness is defined by the parameter δ. This external region is instrumental in averting noise-induced chattering when switching between the MRP triplets [13]. Similar to δ, selecting α must ensure that no measurement disturbance results in an ambiguous choice of the quaternion. Bearing in mind (2) and the definition of $\tilde{\mathbf{R}}$, the kinematic equation for the MRP error representation has the form

$$\dot{\tilde{\boldsymbol{\vartheta}}} = \mathbf{T}(\tilde{\boldsymbol{\vartheta}})\tilde{\boldsymbol{\omega}} = \mathbf{T}(\tilde{\boldsymbol{\vartheta}})(\boldsymbol{\omega} - \tilde{\mathbf{R}}^\top \boldsymbol{\omega}_\mathbf{d}),$$

where $\tilde{\boldsymbol{\omega}} \in \mathbb{R}^3$ denotes the angular velocity error. Let the control input $\boldsymbol{\tau} \in \mathbb{R}^3$ be defined as follows:

$$\boldsymbol{\tau} = -k_\vartheta \tilde{\boldsymbol{\vartheta}}_\mathbf{f} - k_\omega \tilde{\boldsymbol{\omega}} + \boldsymbol{\tau}_\mathbf{c} - \boldsymbol{\zeta},$$

with $k_\vartheta, k_\omega \in \mathbb{R}_{>0}$ and where $\boldsymbol{\tau}_\mathbf{c} \in \mathbb{R}^3$ is given by

$$\boldsymbol{\tau}_\mathbf{c} := -\left[\mathbf{J}\boldsymbol{\omega}\right]_\times \boldsymbol{\omega} + \mathbf{J}(\tilde{\mathbf{R}}^\top \dot{\boldsymbol{\omega}}_\mathbf{d} - \left[\tilde{\boldsymbol{\omega}}\right]_\times \tilde{\mathbf{R}}^\top \boldsymbol{\omega}_\mathbf{d}),$$

and $\boldsymbol{\zeta} \in \mathbb{R}^3$ is an integral term, included to estimate the disturbance $\mathbf{d}$, satisfying

$$\dot{\boldsymbol{\zeta}} := 2^{-1} k_\zeta (\boldsymbol{\Lambda}_{\boldsymbol{\vartheta}} \tilde{\boldsymbol{\vartheta}} + \boldsymbol{\Lambda}_{\boldsymbol{\omega}} \tilde{\boldsymbol{\omega}}),$$

with $k_\zeta \in \mathbb{R}_{>0}$ and $\boldsymbol{\Lambda}_{\boldsymbol{\vartheta}}, \boldsymbol{\Lambda}_{\boldsymbol{\vartheta}} \in \mathbb{R}^{3\times3}_{\succ 0}$ verifying

$$\boldsymbol{\Lambda}_{\boldsymbol{\vartheta}} := \operatorname{diag}(\dot{\boldsymbol{\sigma}}(\mathbf{J}\tilde{\boldsymbol{\omega}})) - k_\vartheta \mathbf{E}, \quad \boldsymbol{\Lambda}_{\boldsymbol{\omega}} := 2c\mathbf{I_3} - k_\omega \mathbf{E},$$

where $c \in \mathbb{R}_{>0}$, $\boldsymbol{\sigma}$ is a saturation function conforming to Definition 1, and $\mathbf{E} \in \mathbb{R}^{3\times3}$ is a negative-definite matrix:

$$\mathbf{E} := -k_\omega k_\zeta^{-1} (\lambda_{\max}(\mathbf{J})\mathbf{J})^{-1/2}.$$

In addition, $\tilde{\boldsymbol{\vartheta}}_\mathbf{f} \in \mathbb{R}^3$ is a continuous dynamical state that is the output of the first-order linear filter

$$\dot{\tilde{\boldsymbol{\vartheta}}}_\mathbf{f} := -k_f(\tilde{\boldsymbol{\vartheta}}_\mathbf{f} - \tilde{\boldsymbol{\vartheta}}), \tag{9}$$

with $k_f \in \mathbb{R}_{>0}$, that has $\tilde{\boldsymbol{\vartheta}}$ as a bounded discontinuous input. The inclusion of this first-order system in the control architecture enables transferring the discrete jumps of $\tilde{\boldsymbol{\vartheta}}$ one integrator away from the control action [6]. Consequently, the torque input becomes continuous due to this relocation of the MRP discontinuities. Define the state-space $\boldsymbol{\chi}_{\boldsymbol{\vartheta}} = \boldsymbol{\Omega} \times (1+\delta)\mathbb{B}^3 \times \mathbb{R}^3 \times \mathbb{R}^3 \times \mathbb{R}^3$ and the state $\mathbf{x}_{\boldsymbol{\vartheta}} := (\mathbf{r}, \tilde{\boldsymbol{\vartheta}}, \tilde{\boldsymbol{\omega}}, \boldsymbol{\zeta}, \tilde{\boldsymbol{\vartheta}}_\mathbf{f}) \in \boldsymbol{\chi}_{\boldsymbol{\vartheta}}$. Then, the closed-loop hybrid attitude tracking system in the covering space $\mathcal{H}_{\boldsymbol{\vartheta}} = (\mathbf{C}_{\boldsymbol{\vartheta}}, \mathbf{F}_{\boldsymbol{\vartheta}}, \mathbf{D}_{\boldsymbol{\vartheta}}, \mathbf{G}_{\boldsymbol{\vartheta}})$ is defined by

$$\mathbf{C}_{\boldsymbol{\vartheta}}(\mathbf{x}_{\boldsymbol{\vartheta}}) := \{\mathbf{x}_{\boldsymbol{\vartheta}} \in \boldsymbol{\chi}_{\boldsymbol{\vartheta}} : \|\tilde{\boldsymbol{\vartheta}}\| \leq 1 + \delta\}$$

$$
\mathbf{F}_{\boldsymbol{\vartheta}}(\mathbf{x}_{\boldsymbol{\vartheta}}) := \begin{pmatrix} \mathbf{F}_{\mathbf{r}}(\mathbf{r}) \\ \mathbf{T}(\tilde{\boldsymbol{\vartheta}})\tilde{\boldsymbol{\omega}} \\ \mathbf{J}^{-1}(-k_\vartheta \tilde{\boldsymbol{\vartheta}}_{\mathbf{f}} - k_\omega \tilde{\boldsymbol{\omega}} + \mathbf{d} - \boldsymbol{\zeta}) \\ 2^{-1}k_\zeta(\boldsymbol{\Lambda}_{\boldsymbol{\vartheta}}\tilde{\boldsymbol{\vartheta}} + \boldsymbol{\Lambda}_{\boldsymbol{\omega}}\tilde{\boldsymbol{\omega}}) \\ -k_f(\tilde{\boldsymbol{\vartheta}}_{\mathbf{f}} - \tilde{\boldsymbol{\vartheta}}) \end{pmatrix}
$$

$$
\mathbf{D}_{\boldsymbol{\vartheta}}(\mathbf{x}_{\boldsymbol{\vartheta}}) := \{\mathbf{x}_{\boldsymbol{\vartheta}} \in \boldsymbol{\chi}_{\boldsymbol{\vartheta}} : \|\tilde{\boldsymbol{\vartheta}}\| = 1 + \delta\}
$$

$$
\mathbf{G}_{\boldsymbol{\vartheta}}(\mathbf{x}_{\boldsymbol{\vartheta}}) := (\mathbf{r}, \boldsymbol{\Upsilon}(\tilde{\boldsymbol{\vartheta}}), \tilde{\boldsymbol{\omega}}, \boldsymbol{\zeta}, \tilde{\boldsymbol{\vartheta}}_{\mathbf{f}})
$$

Let $\tilde{\mathbf{x}}_{\boldsymbol{\vartheta}} := (\tilde{\boldsymbol{\vartheta}}, \tilde{\boldsymbol{\omega}}, \tilde{\mathbf{d}}, \mathbf{e}_{\boldsymbol{\vartheta}}) \in (1+\delta)\mathbb{B}^3 \times \mathbb{R}^3 \times \mathbb{R}^3 \times \mathbb{R}^3$, with $\tilde{\mathbf{d}} := \mathbf{d} - \boldsymbol{\zeta}$ and $\mathbf{e}_{\boldsymbol{\vartheta}} := \tilde{\boldsymbol{\vartheta}}_{\mathbf{f}} - \tilde{\boldsymbol{\vartheta}}$. Theorem 1 demonstrates the stability results of the set $\mathcal{A}_\vartheta := \{\mathbf{x}_{\boldsymbol{\vartheta}} \in \boldsymbol{\chi}_{\boldsymbol{\vartheta}} : \tilde{\mathbf{x}}_{\boldsymbol{\vartheta}} = \mathbf{0}\}$ for the hybrid system $\mathcal{H}_{\boldsymbol{\vartheta}}$.

Theorem 1: Let c and k_f verify the conditions:

$$
c > \max\left\{\frac{\lambda_{\max}(\mathbf{J})}{(2(1+\alpha_\vartheta^2))^{-1}k_\omega} + \frac{k_\omega^2}{k_\zeta \lambda_{\min}(\mathbf{J})}, \frac{\alpha_\delta}{k_\vartheta} + \frac{k_\omega^2}{4k_\zeta \lambda_{\max}(\mathbf{J})}\right\} \tag{11a}
$$

$$
c > \max\left\{\frac{\sqrt{\alpha_\vartheta}\lambda_{\max}(\mathbf{J})}{\sqrt{3k_\vartheta \ln(1+\alpha_\vartheta^2)\lambda_{\min}(\mathbf{J})}}, 2\frac{k_\omega}{k_\vartheta}\right\} \tag{11b}
$$

$$
k_f > \max\left\{\frac{3k_\vartheta}{4f}, \frac{3k_\omega k_\vartheta^2}{8fk_\zeta}\left(\frac{\lambda_{\min}(\mathbf{J})^{-1}}{\lambda_{\max}(\mathbf{J})}\right)^{\frac{1}{2}}, \frac{3(4ck_\vartheta + f(1+\alpha_\vartheta^2)^2)}{2cfk_\omega}\right\} \tag{11c}
$$

with $\alpha_\vartheta = 1 + \delta$, $f \in \mathbb{R}_{>0}$, and

$$
\alpha_\delta = \frac{\delta + \frac{1}{\alpha_\vartheta^2}\left((\alpha_\vartheta^2 - 1)\alpha_\vartheta\sqrt{3}M + f(1 + 2\alpha_f\alpha_\vartheta(1+\alpha_\vartheta^2))\right)}{\ln(\alpha_\vartheta)},
$$

where $\alpha_f = \|\tilde{\boldsymbol{\vartheta}}_{\mathbf{f}}(0,0)\| + \alpha_\vartheta$. Then, $\mathcal{A}_\vartheta$ is uniformly globally asymptotically stable for $\mathcal{H}_{\boldsymbol{\vartheta}}$ and the number of jumps is bounded. Furthermore, for every compact set $\boldsymbol{\Omega}_{\boldsymbol{\vartheta}} \subset \boldsymbol{\chi}_{\boldsymbol{\vartheta}}$ and every $\mathbf{x}_{\boldsymbol{\vartheta}}(0,0) \in \boldsymbol{\Omega}_{\boldsymbol{\vartheta}}$, $\mathcal{A}_\vartheta$ is exponentially stable for $\mathcal{H}_{\boldsymbol{\vartheta}}$.

Proof: Define the Lyapunov function $V(\mathbf{x}_{\boldsymbol{\vartheta}}) : \boldsymbol{\chi}_{\boldsymbol{\vartheta}} \mapsto \mathbb{R}_{\geq 0}$

$$
\begin{aligned}
V(\mathbf{x}_{\boldsymbol{\vartheta}}) = {} & 2a\ln(1 + \|\tilde{\boldsymbol{\vartheta}}\|^2) + \tilde{\boldsymbol{\vartheta}}^\top \boldsymbol{\sigma}(\mathbf{J}\tilde{\boldsymbol{\omega}}) + c\tilde{\boldsymbol{\omega}}^\top \mathbf{J}\tilde{\boldsymbol{\omega}} \\
& + \tfrac{1}{k_\zeta}\|\tilde{\mathbf{d}}\|^2 + \tilde{\mathbf{d}}^\top \mathbf{E}\mathbf{J}\tilde{\boldsymbol{\omega}} + f\|\mathbf{e}_{\boldsymbol{\vartheta}}\|^2,
\end{aligned}
$$

where $a \in \mathbb{R}_{>0}$ satisfies $a = 2ck_\vartheta - k_\omega^2 k_\vartheta (2k_\zeta \lambda_{\max}(\mathbf{J}))^{-1} > 0$. The function V is radially unbounded and continuously differentiable on $\boldsymbol{\chi}_{\boldsymbol{\vartheta}}$. Hence, for any given $\mathbf{x}_{\boldsymbol{\vartheta}}(0,0)$, the set $\mathbf{U} = \{\mathbf{x}_{\boldsymbol{\vartheta}} \in \boldsymbol{\chi}_{\boldsymbol{\vartheta}} : V(\mathbf{x}_{\boldsymbol{\vartheta}}) \leq V(\mathbf{x}_{\boldsymbol{\vartheta}}(0,0))\}$ is compact. Since $\mathbf{x}_{\boldsymbol{\vartheta}} \in \mathbf{C}_\vartheta$ implies $\|\tilde{\boldsymbol{\vartheta}}\| \leq \alpha_\vartheta$, the inequality $\ln(1 + \|\tilde{\boldsymbol{\vartheta}}\|^2) \geq \ln(1+\alpha_\vartheta^2)\alpha_\vartheta^{-2}\|\tilde{\boldsymbol{\vartheta}}\|^2$ holds during flows. In this direction, for $\mathbf{x}_{\boldsymbol{\vartheta}} \in \mathbf{C}_\vartheta$, V obeys the lower-bound

$$
\begin{aligned}
V(\mathbf{x}_{\boldsymbol{\vartheta}}) \geq {} & 2a\ln(1+\alpha_\vartheta^2)\alpha_\vartheta^{-2}\|\tilde{\boldsymbol{\vartheta}}\|^2 - \lambda_{\max}(\mathbf{J})\|\tilde{\boldsymbol{\vartheta}}\|\|\tilde{\boldsymbol{\omega}}\| + f\|\mathbf{e}_{\boldsymbol{\vartheta}}\|^2 \\
& + k_\zeta^{-1}\|\tilde{\mathbf{d}}\|^2 - k_\omega k_\zeta^{-1}\|\tilde{\mathbf{d}}\|\|\tilde{\boldsymbol{\omega}}\| + c\lambda_{\min}(\mathbf{J})\|\tilde{\boldsymbol{\omega}}\|^2,
\end{aligned}
$$

which leads to $V(\tilde{\mathbf{x}}_{\boldsymbol{\vartheta}}) \geq \lambda_{\min}(\mathbf{A_1})\|\mathbf{x}_{\boldsymbol{\vartheta}}\|$ with

$$
\mathbf{A_1} = \frac{1}{2}\begin{bmatrix} 4a\ln(1+\alpha_\vartheta^2)\alpha_\vartheta^{-2} & -\lambda_{\max}(\mathbf{J}) & 0 & 0 \\ -\lambda_{\max}(\mathbf{J}) & 2c\lambda_{\min}(\mathbf{J}) & -k_\omega k_\zeta^{-1} & 0 \\ 0 & -k_\omega k_\zeta^{-1} & 2k_\zeta^{-1} & 0 \\ 0 & 0 & 0 & 2f \end{bmatrix}.
$$

Given (11a) and (11b), $\mathbf{A_1}$ is positive definite and, consequently, the function V is positive definite with respect to $\mathcal{A}_\vartheta$. In addition, V also verifies the upper-bound $V(\mathbf{x}_{\boldsymbol{\vartheta}}) \leq \lambda_{\max}(\mathbf{A_2})\|\tilde{\mathbf{x}}_{\boldsymbol{\vartheta}}\|$ with $\mathbf{A_2} \in \mathbb{R}^{4\times 4}_{\succ 0}$ given by

$$
\mathbf{A_2} = \frac{1}{2}\begin{bmatrix} 4a & \lambda_{\max}(\mathbf{J}) & 0 & 0 \\ \lambda_{\max}(\mathbf{J}) & 2c\lambda_{\max}(\mathbf{J}) & k_\omega k_\zeta^{-1} & 0 \\ 0 & k_\omega k_\zeta{-1} & 2k_\zeta^{-1} & 0 \\ 0 & 0 & 0 & 2f \end{bmatrix}.
$$

By virtue of (11a) and given $4\tilde{\boldsymbol{\vartheta}}^\top \mathbf{T}(\tilde{\boldsymbol{\vartheta}}) = (1+\|\tilde{\boldsymbol{\vartheta}}\|^2)\tilde{\boldsymbol{\vartheta}}^\top$ for all $\tilde{\boldsymbol{\vartheta}} \in \mathbb{R}^3$, the bound $\|\tilde{\boldsymbol{\vartheta}}\| \leq \alpha_\vartheta$ and the equality [15, p. 123]

$$
\mathbf{T}(\tilde{\boldsymbol{\vartheta}})^\top \mathbf{T}(\tilde{\boldsymbol{\vartheta}}) = 4^{-2}(1 + \|\tilde{\boldsymbol{\vartheta}}\|^2)^2 \mathbf{I_3}, \tag{12}
$$

which leads to $\|\mathbf{T}(\tilde{\boldsymbol{\vartheta}})\| \leq 4^{-1}(1+\alpha_\vartheta^2)$, one has

$$
\begin{aligned}
\dot{V}(\mathbf{x}_{\boldsymbol{\vartheta}}) \leq {} & -k_\vartheta \tilde{\boldsymbol{\vartheta}}^\top \boldsymbol{\Theta}\tilde{\boldsymbol{\vartheta}} - \tilde{\boldsymbol{\vartheta}}^\top k_\omega \boldsymbol{\Theta}^* \tilde{\boldsymbol{\omega}} + \tilde{\mathbf{d}}^\top \mathbf{E}\tilde{\mathbf{d}} \\
& - \tfrac{ck_\omega}{2}\|\tilde{\boldsymbol{\omega}}\|^2 - 2fk_f\|\mathbf{e}_{\boldsymbol{\vartheta}}\|^2 - k_\vartheta \tilde{\mathbf{d}}^\top \mathbf{E}\mathbf{e}_{\boldsymbol{\vartheta}} \\
& - k_\vartheta \tilde{\boldsymbol{\vartheta}}^\top \boldsymbol{\Theta}\mathbf{e}_{\boldsymbol{\vartheta}} + \tfrac{1}{2}(4ck_\vartheta + f(1+\alpha_\vartheta^2))\|\mathbf{e}_{\boldsymbol{\vartheta}}\|\|\tilde{\boldsymbol{\omega}}\|,
\end{aligned}
$$

where $\boldsymbol{\Theta} = \operatorname{diag}(\dot{\boldsymbol{\sigma}}_{\boldsymbol{\vartheta}}(\mathbf{J}\tilde{\boldsymbol{\omega}}))$ and

$$
\boldsymbol{\Theta}^* = \boldsymbol{\Theta} - (2\sqrt{\lambda_{\max}(\mathbf{J})})^{-1}\boldsymbol{\Theta}\mathbf{J}^{\frac{1}{2}} \preceq \boldsymbol{\Theta}.
$$

Note that the function $\dot{V}$ is negative definite if the matrices

$$
\mathbf{C_1} = \begin{bmatrix} k_\vartheta \boldsymbol{\Theta} & k_\omega \boldsymbol{\Theta} \\ k_\omega \boldsymbol{\Theta} & \frac{ck_\omega}{2}\mathbf{I_3} \end{bmatrix}, \mathbf{C_2} = \begin{bmatrix} k_\vartheta \boldsymbol{\Theta} & k_\vartheta \boldsymbol{\Theta} \\ k_\vartheta \boldsymbol{\Theta} & \frac{4fk_f}{3}\mathbf{I_3} \end{bmatrix}, \mathbf{C_3} = \begin{bmatrix} -2\mathbf{E} & k_\vartheta \mathbf{E} \\ k_\vartheta \mathbf{E} & \frac{8fk_f}{3}\mathbf{I_3} \end{bmatrix},
$$

$$
\text{and } \mathbf{C_4} = \begin{bmatrix} ck_\omega & 4ck_\vartheta + (1+\alpha_\vartheta^2) \\ 4ck_\vartheta + (1+\alpha_\vartheta^2) & \frac{8fk_f}{3} \end{bmatrix}
$$

are positive definite. Considering Definition 1, (11b), and (11c), for each one of the previous matrices, the upper-left submatrix and its respective Schur complement are positive definite. Thus, it follows that $\dot{V} \leq -W_f(\mathbf{x}_{\boldsymbol{\vartheta}})$, with $W_f(\mathbf{x}_{\boldsymbol{\vartheta}}) : \boldsymbol{\chi}_{\boldsymbol{\vartheta}} \mapsto \mathbb{R}_{\geq 0}$ being a positive definite function with respect to $\mathcal{A}_\vartheta$. Between jumps, V verifies

$$
\begin{aligned}
V(\mathbf{G}_{\boldsymbol{\vartheta}}(\mathbf{x}_{\boldsymbol{\vartheta}})) - V(\mathbf{x}_{\boldsymbol{\vartheta}}) = {} & -4a\ln(\|\tilde{\boldsymbol{\vartheta}}\|) + \|\tilde{\boldsymbol{\vartheta}}\|^{-2} - \|\tilde{\boldsymbol{\vartheta}}\|^2 \\
& + f(1 + \|\tilde{\boldsymbol{\vartheta}}\|^{-2})(2\tilde{\boldsymbol{\vartheta}}_{\mathbf{f}}^\top \tilde{\boldsymbol{\vartheta}} - b\tilde{\boldsymbol{\vartheta}}^\top \boldsymbol{\sigma}_{\boldsymbol{\vartheta}}(\mathbf{J}\tilde{\boldsymbol{\omega}})).
\end{aligned}
$$

Since $\tilde{\boldsymbol{\vartheta}}_{\mathbf{f}}$ results from a first-order linear filter with $\tilde{\boldsymbol{\vartheta}}$ as input, $\|\tilde{\boldsymbol{\vartheta}}_{\mathbf{f}}(t,j)\| \leq \alpha_f \;\; \forall \;\; (t,j) \in \operatorname{dom} \mathbf{x}_{\boldsymbol{\vartheta}}$. Combining (11a) with the bound $\|\tilde{\boldsymbol{\vartheta}}\| \leq \alpha_\vartheta \;\; \forall \;\; \mathbf{x}_{\boldsymbol{\vartheta}} \in \boldsymbol{\chi}_{\boldsymbol{\vartheta}}$ leads to $V(\mathbf{G}_{\boldsymbol{\vartheta}}(\mathbf{x}_{\boldsymbol{\vartheta}})) - V(\mathbf{x}_{\boldsymbol{\vartheta}}) \leq -\delta$. Thus, there exists a continuous function $W_j(\mathbf{x}_{\boldsymbol{\vartheta}}) : \boldsymbol{\chi}_{\boldsymbol{\vartheta}} \mapsto \mathbb{R}_{\geq 0}$ that is positive definite with respect to $\mathcal{A}_\vartheta$ such that $V(\mathbf{G}_{\boldsymbol{\vartheta}}(\mathbf{x}_{\boldsymbol{\vartheta}})) - V(\mathbf{x}_{\boldsymbol{\vartheta}}) \leq -W_j(\mathbf{x}_{\boldsymbol{\vartheta}})$. Hence, V strictly decreases during both jumps and flows. Consequently, any solution $\mathbf{x}_{\boldsymbol{\vartheta}}(t, j)$ to $\mathcal{H}_{\boldsymbol{\vartheta}}$ remains in $\mathbf{U}$ for all $(t,j) \in \operatorname{dom} \mathbf{x}_{\boldsymbol{\vartheta}}$ and, since $\mathbf{G}_{\boldsymbol{\vartheta}}(\mathbf{D}_{\boldsymbol{\vartheta}}) \subset \mathbf{C}_{\boldsymbol{\vartheta}}$, does not jump out of $\mathbf{C} \cup \mathbf{D}$. Thus, any maximal solution to $\mathcal{H}_{\boldsymbol{\vartheta}}$ [17, Definition 2.7] is bounded and complete [17, Proposition 6.10]. Furthermore, the number of jumps is bounded by

$$
j \leq J = \delta^{-1}V(\mathbf{x}_{\boldsymbol{\vartheta}}(0,0))
$$

and, based on [17, Theorem 3.18], $\mathcal{A}_\vartheta$ is uniformly globally asymptotically stable for $\mathcal{H}_{\boldsymbol{\vartheta}}$. Since any solution $\mathbf{x}_{\boldsymbol{\vartheta}}(t, j)$ to $\mathcal{H}_{\boldsymbol{\vartheta}}$ remains in $\mathbf{U}$ for all $(t,j) \in \operatorname{dom} \mathbf{x}_{\boldsymbol{\vartheta}}$, V satisfies $\dot{V} \leq -\alpha_{\dot{V}}\|\tilde{\mathbf{x}}_{\boldsymbol{\vartheta}}\|^2 \;\; \forall \;\; \mathbf{x}_{\boldsymbol{\vartheta}} \in \mathbf{C}_{\boldsymbol{\vartheta}}$ with

$$
\alpha_{\dot{V}} = \inf_{\mathbf{x}_{\boldsymbol{\vartheta}} \in \mathbf{U}} \lambda_{\min}(\mathbf{B}(\mathbf{x}_{\boldsymbol{\vartheta}}))
$$

$$
\mathbf{B} = \frac{1}{4}\begin{bmatrix} 4k_\vartheta \boldsymbol{\Theta} & 2k_\omega \boldsymbol{\Theta}^* & \mathbf{0} & 2k_\vartheta \boldsymbol{\Theta} \\ 2k_\omega \boldsymbol{\Theta}^* & 2ck_\omega \mathbf{I_3} & \mathbf{0} & 4ck_\vartheta + f + f\alpha_\vartheta^2 \\ \mathbf{0} & \mathbf{0} & -\mathbf{E} & 2k_\vartheta \mathbf{E} \\ 2k_\vartheta \boldsymbol{\Theta} & 4ck_\vartheta + f + f\alpha_\vartheta^2 & 2k_\vartheta \mathbf{E} & 8fk_f \mathbf{I_3} \end{bmatrix},
$$

and

$$
V(\mathbf{G}_{\boldsymbol{\vartheta}}(\mathbf{x}_{\boldsymbol{\vartheta}})) \leq e^{-\alpha_\delta}V(\mathbf{x}_{\boldsymbol{\vartheta}}) \quad \forall \quad \mathbf{x}_{\boldsymbol{\vartheta}} \in \mathbf{D}_{\boldsymbol{\vartheta}}, \tag{13}
$$

with $\alpha_\delta = -\ln(1 - \delta/\max\{V(0,0), 2\delta\})$. Note that $\mathbf{B}$ is positive definite for any $\tilde{\boldsymbol{\omega}} \in \mathbb{R}^3$, yielding $\alpha_{\dot{V}} \in \mathbb{R}_{>0}$. In this way, one has

$$
\dot{V} \leq -\lambda_\vartheta V \quad \forall \quad \mathbf{x}_{\boldsymbol{\vartheta}} \in \mathbf{C}_{\boldsymbol{\vartheta}} \tag{14a}
$$

$$
V(\mathbf{G}_{\boldsymbol{\vartheta}}(\mathbf{x}_{\boldsymbol{\vartheta}})) \leq e^{-\lambda_\vartheta}V(\mathbf{x}_{\boldsymbol{\vartheta}}) \quad \forall \quad \mathbf{x}_{\boldsymbol{\vartheta}} \in \mathbf{D}_{\boldsymbol{\vartheta}}, \tag{14b}
$$

with $\lambda_\vartheta = \min\{\alpha_{\dot{V}}^{-1}\lambda_{\max}(\mathbf{A_2}), \alpha_\delta\}$. Therefore, based on [18, Theorem 1], for every compact set $\boldsymbol{\Omega}_{\boldsymbol{\vartheta}} \subset \boldsymbol{\chi}_{\boldsymbol{\vartheta}}$ and every $\mathbf{x}_{\boldsymbol{\vartheta}}(0,0) \in \boldsymbol{\Omega}_{\boldsymbol{\vartheta}}$, $\mathcal{A}_\vartheta$ is robustly globally asymptotically stable and robustly semi-globally exponentially stable for $\mathcal{H}_{\boldsymbol{\vartheta}}$. ■

Remark 1: Since λ_ϑ depends on $\mathbf{x}_{\boldsymbol{\vartheta}}(0,0) \in \boldsymbol{\Omega}_{\boldsymbol{\vartheta}}$, with $\boldsymbol{\Omega}_{\boldsymbol{\vartheta}}$ denoting an arbitrarily large compact set, the exponential stability result in Theorem 1 holds semi-globally. □

Remark 2: The constant f, featured in conditions (11a) and (11c), can be arbitrarily defined with a positive value. Its incorporation offers some flexibility in selecting k_f and c by increasing the preponderance of $\|\mathbf{e}_{\boldsymbol{\vartheta}}\|^2$ in $V(\mathbf{x}_{\boldsymbol{\vartheta}})$. □

V. Robust Global Exponential Tracking on SO(3)

This section resorts to the equivalence of stability concepts developed in [14] to obtain a robust tracking result in the base space $\mathrm{SO}(3)$ with the dynamic feedback controller designed in the covering space. Let $\mathcal{H}_{\mathbf{R}} := (\mathbf{C}_{\mathbf{R}}, \mathbf{F}_{\mathbf{R}}, \mathbf{D}_{\mathbf{R}}, \mathbf{G}_{\mathbf{R}})$ represent the closed-loop hybrid system encapsulating the reference trajectory and the interconnection between the attitude tracking dynamics described in the base space $\mathrm{SO}(3)$, the dynamic path lifting algorithm $\mathcal{H}_{\mathbf{l}}$, and the dynamics and output of the MRP-based feedback controller previously designed. Define the state-space $\boldsymbol{\chi}_{\mathbf{R}} = \boldsymbol{\Omega} \times \boldsymbol{\chi}_{\mathbf{l}} \times \mathbb{R}^3 \times \mathbb{R}^3 \times \mathbb{R}^3$ and state-vector $\mathbf{x}_{\mathbf{R}} := (\mathbf{r}, \mathbf{x}_{\mathbf{l}}, \tilde{\boldsymbol{\omega}}, \boldsymbol{\zeta}, \tilde{\boldsymbol{\vartheta}}_{\mathbf{f}})$. The quadruplet

$$\mathbf{C}_{\mathbf{R}}(\mathbf{x}_{\mathbf{R}}) := \{\mathbf{x}_{\mathbf{R}} \in \boldsymbol{\chi}_{\mathbf{R}} : \mathbf{x}_{\mathbf{l}} \in \mathbf{C}_{\mathbf{l}} \cap \mathbf{C}_{\mathbf{m}}\}$$

$$\mathbf{F}_{\mathbf{R}}(\mathbf{x}_{\mathbf{R}}) := \begin{pmatrix} \mathbf{F}_{\mathbf{r}}(\mathbf{r}) \\ \mathbf{0} \\ 0 \\ \tilde{\mathbf{R}}\,[\tilde{\boldsymbol{\omega}}]_\times \\ \mathbf{J}^{-1}(-k_\vartheta \tilde{\boldsymbol{\vartheta}}_{\mathbf{f}} - k_\omega \tilde{\boldsymbol{\omega}} + \mathbf{d} - \boldsymbol{\zeta}) \\ 2^{-1} k_\zeta (\boldsymbol{\Lambda}_{\boldsymbol{\vartheta}} \boldsymbol{\varphi}(m\boldsymbol{\Phi}(\hat{\mathbf{q}}, \tilde{\mathbf{R}})) + \boldsymbol{\Lambda}_{\boldsymbol{\omega}} \tilde{\boldsymbol{\omega}}) \\ -k_f(\tilde{\boldsymbol{\vartheta}}_{\mathbf{f}} - \boldsymbol{\varphi}(m\boldsymbol{\Phi}(\hat{\mathbf{q}}, \tilde{\mathbf{R}}))) \end{pmatrix}$$

$$\mathbf{D}_{\mathbf{R}}(\mathbf{x}_{\mathbf{R}}) := \{\mathbf{x}_{\mathbf{R}} \in \boldsymbol{\chi}_{\mathbf{R}} : \mathbf{x}_{\mathbf{l}} \in \mathbf{D}_{\mathbf{m}} \cup \mathbf{D}_{\mathbf{l}}\}$$

$$\mathbf{G}_{\mathbf{R}}(\mathbf{x}_{\mathbf{R}}) := \begin{cases} (\mathbf{r}, \boldsymbol{\Phi}(\hat{\mathbf{q}}, \tilde{\mathbf{R}}), m, \tilde{\mathbf{R}}, \tilde{\boldsymbol{\omega}}, \boldsymbol{\zeta}, \tilde{\boldsymbol{\vartheta}}_{\mathbf{f}}), & \mathbf{x}_{\mathbf{l}} \in \mathbf{D}_{\mathbf{l}} \\ (\mathbf{r}, \hat{\mathbf{q}}, -m, \tilde{\mathbf{R}}, \tilde{\boldsymbol{\omega}}, \boldsymbol{\zeta}, \tilde{\boldsymbol{\vartheta}}_{\mathbf{f}}) & , \mathbf{x}_{\mathbf{l}} \in \mathbf{D}_{\mathbf{m}} \end{cases}$$

characterizes $\mathcal{H}_{\mathbf{R}}$. Theorem 2 presents the main result of this paper: the MRP-based dynamic hybrid feedback yields equivalent stability properties for $\mathcal{H}_{\mathbf{R}}$. Additionally, the next theorem also demonstrates the robustness of this result.

Theorem 2: The hybrid system $\mathcal{H}_{\mathbf{R}}$ is well-posed. Furthermore, the set $\mathcal{A}_R := \{\mathbf{x}_{\mathbf{R}} \in \boldsymbol{\chi}_{\mathbf{R}} : \tilde{\mathbf{R}} = \mathbf{I}_3, \tilde{\boldsymbol{\omega}} = \mathbf{0}, \tilde{\mathbf{d}} = \mathbf{0}, \mathbf{e}_{\boldsymbol{\vartheta}} = \mathbf{0}\}$ is robustly globally asymptotically stable and semi-globally exponentially stable for $\mathcal{H}_{\mathbf{R}}$.

Proof: The autonomous hybrid system $\mathcal{H}_{\mathbf{l}}$ is well-posed [14]. The sets $\mathbf{C}_{\mathbf{R}}$ and $\mathbf{D}_{\mathbf{R}}$ are closed subsets of $\boldsymbol{\chi}_{\mathbf{R}}$. The flow map $\mathbf{F}_{\mathbf{R}}(\mathbf{x}_{\mathbf{R}})$ comprises a convex and bounded map and continuous differential equations. Therefore, $\mathbf{F}_{\mathbf{R}}(\mathbf{x}_{\mathbf{R}})$ is locally bounded relative to $\mathbf{C}_{\mathbf{R}}(\mathbf{x}_{\mathbf{R}}) \subset \operatorname{dom} \mathbf{F}_{\mathbf{R}}$ and outer semicontinuous, and $\mathbf{F}_{\mathbf{R}}(\mathbf{x}_{\mathbf{R}})$ is convex for every $\mathbf{x}_{\mathbf{R}} \in \mathbf{C}_{\mathbf{R}}$. Moreover, since $\mathbf{r}, \tilde{\mathbf{R}}, \tilde{\boldsymbol{\omega}}, \boldsymbol{\zeta}$, and $\tilde{\boldsymbol{\vartheta}}_{\mathbf{f}}$ remain constant during jumps, the respective difference equations are continuous. Thus, since $\mathcal{H}_{\mathbf{l}}$ is well-posed, $\mathbf{G}_{\mathbf{R}}(\mathbf{x}_{\mathbf{R}})$ is outer semicontinuous and locally bounded relative to $\mathbf{D}_{\mathbf{R}}(\mathbf{x}_{\mathbf{R}}) \subset \operatorname{dom} \mathbf{G}_{\mathbf{R}}$. Consequently, $\mathcal{H}_{\mathbf{R}}$ verifies the hybrid basic conditions [17, Assumption 6.5] and is well-posed [17, Theorem 6.30].

Based on Theorem 1, for all $\mathbf{x}_{\boldsymbol{\vartheta}}(0,0) \in \mathcal{B}_{\boldsymbol{\vartheta}} = \boldsymbol{\chi}_{\boldsymbol{\vartheta}}$, the set $\mathcal{A}_\vartheta$ is asymptotically stable for $\mathcal{H}_{\boldsymbol{\vartheta}}$. Then, it follows from [14, Theorem 1 and Lemma 2] and (3), that $\mathcal{A}_R$ is asymptotic stable for $\mathcal{H}_{\mathbf{R}}$ with $\{\mathbf{x}_{\mathbf{R}} \in \boldsymbol{\chi}_{\mathbf{R}} : \operatorname{dist}(\hat{\mathbf{q}}, \mathcal{Q}(\tilde{\mathbf{R}})) < 1\}$ as basin of attraction. Theorem 1 also proves that, for any arbitrarily large compact set $\boldsymbol{\Omega}_{\boldsymbol{\vartheta}}$ and any $\mathbf{x}_{\boldsymbol{\vartheta}}(0,0) \in \mathcal{B}_{\boldsymbol{\vartheta}} = \boldsymbol{\Omega}_{\boldsymbol{\vartheta}} \subset \boldsymbol{\chi}_{\boldsymbol{\vartheta}}$, $\mathcal{A}_\vartheta$ is exponentially stable for $\mathcal{H}_{\boldsymbol{\vartheta}}$. Hence, in light of [14, Theorem 2], $\mathcal{A}_R$ is exponentially stable for $\mathcal{H}_{\mathbf{R}}$ for all $\mathbf{x}_{\mathbf{R}}(0,0) \in \mathcal{B} = \{\mathbf{x}_{\boldsymbol{\vartheta}} \in \boldsymbol{\chi}_{\boldsymbol{\vartheta}} : (\boldsymbol{\varphi}(m\boldsymbol{\Phi}(\hat{\mathbf{q}}, \mathbf{R})), \boldsymbol{\omega}, \boldsymbol{\zeta}, \tilde{\boldsymbol{\vartheta}}_{\boldsymbol{f}}) \in \boldsymbol{\Omega}_{\boldsymbol{\vartheta}}, \operatorname{dist}(\hat{\mathbf{q}}, \mathcal{Q}(\mathbf{R})) < 1\}$. Furthermore, by virtue of $\mathcal{H}_{\mathbf{R}}$ being well-posed, the stability results of $\mathcal{A}_R$ for $\mathcal{H}_{\mathbf{R}}$ are robust to small perturbations including measurement disturbances [17, Theorem 7.21.]. The robustness margin to perturbations can be quantified through $\mathcal{KL}$ bounds [17, Definition 7.18.]. Hence, $\mathcal{A}_R$ is robustly globally asymptotically stable and semi-globally exponentially stable for $\mathcal{H}_{\mathbf{R}}$. ■

Remark 3: Note that $\tilde{\mathbf{R}} = \mathbf{I}_3$ and $\tilde{\boldsymbol{\omega}} = \mathbf{0}$ imply, respectively, $\mathbf{R} = \mathbf{R}_{\mathbf{d}}$ and $\boldsymbol{\omega} = \boldsymbol{\omega}_{\mathbf{d}}$. Based on these equalities, it follows from Theorem 2 that the solution designed, encompassing the dynamic MRP-based feedback controller, with output $\boldsymbol{\tau}(\mathbf{r}, \tilde{\mathbf{x}}_{\boldsymbol{\vartheta}})$, and the path-lifting algorithm $\mathcal{H}_{\mathbf{l}}$, robustly globally asymptotically and semi-globally exponentially stabilizes the set $\mathcal{A}$ for the attitude dynamics expressed in (5). Thus, the proposed solution effectively tackles Problem 1. □

VI. Simulation Results

To illustrate the robust global property of the proposed control architecture and the underlying hybrid jump logic, the authors conducted a challenging attitude tracking test in simulation. Having the attitude dynamics and kinematics detailed in (5) at its core, the simulation model considers measurement noise and fixed disturbances, and restricts the torque authority within practical reasonable values. In more detail, the model has a sampling time of 0.01 seconds, defines $\mathbf{J} = \operatorname{diag}(2.24, 2.9, 5.3) \times 10^{-3} [\mathrm{kgm}^2]$ as the inertia matrix, considers the external disturbance $\mathbf{d} = (0.2, -0.1, 0.05)$ [Nm], and constraints the torque actuation with the bounds $|\mathbf{e}_1^\top \boldsymbol{\tau}|, |\mathbf{e}_2^\top \boldsymbol{\tau}| \leq 0.45$[Nm] and $|\mathbf{e}_3^\top \boldsymbol{\tau}| \leq 0.15$ [Nm]. The simulation evaluated the capacity of the solution to accurately track an aggressive trajectory, comprising demanding flip maneuvers and a downward-facing initial condition. The saturation function used was $\sigma(s) = M \tanh(s/M)$, with $M = 1$. For the sake of simplicity, the trajectory definition resorts to Euler angles (roll φ, pitch θ, and yaw ψ):

$$\varphi(t) = -\pi(\sigma(1.5\pi(t-2)) - \sigma(1.5\pi(t-6)) + \sigma(9\pi(t-10)) + 1),$$
$$\theta(t) = 0, \quad \psi(t) = -\pi(\sigma(\pi(t-4)) - \sigma(\pi(t-10))) \text{ [rad]}.$$

The initial attitude was $(\varphi, \theta, \psi)(0) = (-179, 0, 260)[^\circ]$, and the control parameters were $k_\vartheta = 3, k_\omega = 0.15, k_\zeta = 0.1, k_f = 160, c = 850, f = (20\lambda_{\max}(\mathbf{J}))^{-1}$, $\alpha = 0.25$, and $\delta = 0.02$.

The simulation results are depicted in Fig. 1, where the attitude response is also presented in Euler angles to ease its interpretation. The rigid body successfully overcame the initial downward-facing orientation and accurately tracked the reference trajectory, illustrating the global nature of the solution. Focusing on Fig. 1a, for the third side flip command, provided slightly before the instant $t = 10$s, the rigid body initiated the desired maneuver, but did not complete it. This third command required a more extreme maneuver, which, due to the limited control authority, led to the increase of the MRP error until the jump set condition was eventually triggered, causing the rigid body to rotate in the opposite direction. As a result, one can observe in

Fig. 1d that the state m jumped from 1 to -1 and the MRP error presented a coherent discrete evolution. The rigid body followed the reference as long as it represented the shortest available rotation; once an equivalent orientation emerged as the new closest target, the direction of rotation changed accordingly. This behavior evidences that the methodology effectively handles tumbling situations and the *unwinding phenomenon*. Moreover, focusing on Fig. 1c, the solution handled the initial tumbling circumstance by performing the shortest available rotation, corroborating this latter claim.

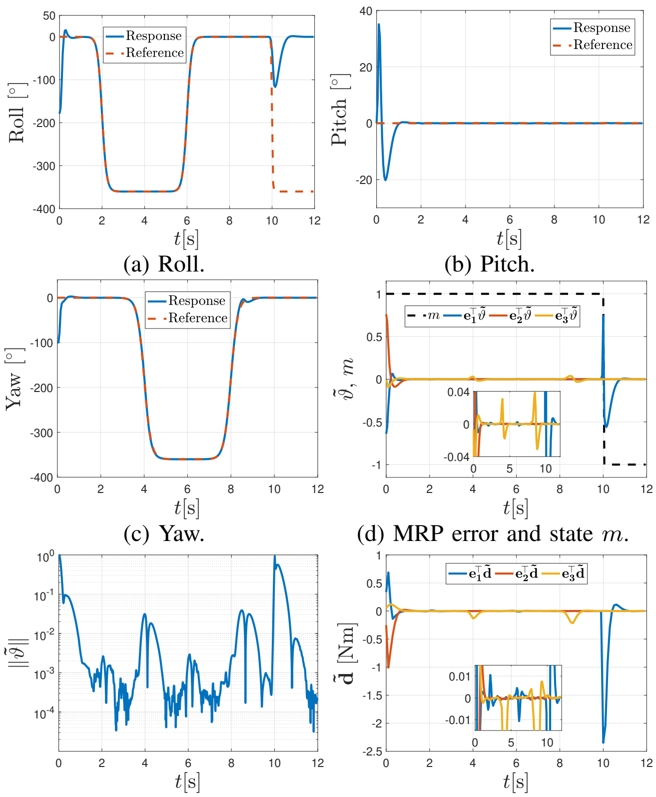

(a) Roll. (b) Pitch.

(c) Yaw. (d) MRP error and state m.

(e) MRP error norm. (f) Disturbance estimation error.

Fig. 1: Attitude responses obtained in simulation.

As shown in Figure 1e, the initial condition led to an MRP error norm just below 1, indicating that the rigid body dealt with the significant initial attitude error by completing the shortest rotation possible. After each side flip, the error norm converged to values smaller than 0.001. Furthermore, the control strategy tracked the first two side flip maneuvers with a maximum MRP error norm of roughly 0.003, highlighting the effectiveness of the global tracking capacity of the hybrid controller. The responses depicted in Figure 1f indicate that the disturbance estimation error $\tilde{\mathrm{d}}$ converged to approximately zero in less than one second. This occurred while the system dealt with the initial downward-facing orientation and after the subsequent flips, contributing to the robust tracking capacity in the presence of a significant fixed disturbance.

VII. Conclusion

The authors designed an MRP-based hybrid dynamic controller with integral action and a smoothing mechanism that outputs a jump-free torque input. The solution renders the attitude dynamics globally asymptotically and semi-globally exponentially stable in the covering space. Furthermore, as the main result, pairing this controller with a hybrid dynamic path-lifting algorithm yields semi-global exponential and global asymptotic tracking results in the attitude configuration manifold $\mathrm{SO}(3)$ with robustness to unknown constant disturbances and small perturbations. The simulation results validate the underlying jump logic and illustrate the global result and capacity to perform aggressive maneuvers accurately in the presence of significant constant disturbances and measurement noise.

VIII. Acknowledgements

The authors acknowledge Fundação para a Ciência e a Tecnologia (FCT) for its financial support via the projects LAETA Base Funding (DOI: 10.54499/UIDB/50022/2020) and LAETA Programatic Funding (DOI: 10.54499/UIDP/50022/2020). Luís Martins holds a PhD scholarship 2022.14126.BD from FCT.

References

[1] N. Chaturvedi, A. Sanyal, and N. McClamroch, "Rigid-body attitude control," *IEEE Control Systems Magazine*, vol.31, no.3, pp.30–51, 2011.

[2] S. Bhat and D. Bernstein, "A topological obstruction to continuous global stabilization of rotational motion and the unwinding phenomenon," *Systems & Control Letters*, vol. 39, no. 1, pp. 63–70, 2000.

[3] T. Lee, "Global exponential attitude tracking controls on $\mathrm{SO}(3)$," *IEEE Transactions on Automatic Control*, vol. 60, no. 10, pp. 2837–2842, 2015.

[4] C. G. Mayhew and A. R. Teel, "On the topological structure of attraction basins for differential inclusions," *Systems & Control Letters*, vol. 60, no. 12, pp. 1045–1050, 2011.

[5] ——, "Synergistic hybrid feedback for global rigid-body attitude tracking on SO (3)*," *IEEE Transactions on Automatic Control*, vol. 58, no. 11, pp. 2730–2742, 2013.

[6] S. Berkane, A. Abdessameud, and A. Tayebi, "Hybrid global exponential stabilization on $\mathrm{SO}(3)$," *Automatica*, vol. 81, pp. 279–285, 2017.

[7] P. Casau, C. G. Mayhew, R. G. Sanfelice, and C. Silvestre, "Robust global exponential stabilization on the n-dimensional sphere with applications to trajectory tracking for quadrotors," *Automatica*, vol. 110, p. 108534, 2019.

[8] M. Wang and A. Tayebi, "Hybrid feedback for global tracking on matrix lie groups $so(3)$ and $se(3)$," *IEEE Transactions on Automatic Control*, vol. 67, no. 6, pp. 2930–2945, 2021.

[9] D. Invernizzi, M. Lovera, and L. Zaccarian, "Global robust attitude tracking with torque disturbance rejection via dynamic hybrid feedback," *Automatica*, vol. 144, p. 110462, 2022.

[10] C. Mayhew, R. Sanfelice, and A. Teel, "On path-lifting mechanisms and unwinding in quaternion-based attitude control," *IEEE Transactions on Automatic Control*, vol. 58, no. 5, pp. 1179–1191, 2013.

[11] L. Martins, C. Cardeira, and P. Oliveira, "Global trajectory tracking for quadrotors: An mrp-based hybrid backstepping strategy," in *60th IEEE Conference on Decision and Control*. IEEE, 2021, pp. 5759–5764.

[12] ——, "Robust global exponential trajectory tracking for quadrotors: An mrp-based hybrid approach," in *62nd IEEE Conference on Decision and Control*. IEEE, 2023, pp. 5249–5254.

[13] ——, "Global trajectory tracking for quadrotors: An mrp-based hybrid strategy with input saturation," *Automatica*, vol. 162, p. 111521, 2024.

[14] ——, "Path-lifting mechanism for mrp and equivalence of stability between results in $\mathbb{R}^3$ and $\mathrm{SO}(3)$," 2023. [Online]. Available: https://arxiv.org/abs/2302.01983

[15] J. L. Junkins and H. Schaub, *Analytical Mechanics of Space Systems*. American Institute of Aeronautics and Astronautics, 2009.

[16] J. Dugundji, *Topology*, 1st ed. Allyn and Bacon, 1966.

[17] R. Goebel, R. G. Sanfelice, and A. Teel, *Hybrid dynamical systems: modeling, stability, and robustness*. Princeton University Press, 2012.

[18] A. R. Teel, F. Forni, and L. Zaccarian, "Lyapunov-based sufficient conditions for exponential stability in hybrid systems," *IEEE Transactions on Automatic Control*, vol. 58, no. 6, pp. 1591–1596, 2012.